

Antiferroelectric and antiferrodistortive phase transitions in Ruddlesden-Popper Pb_2TiO_4 from first-principles

Tao Xu^{*1}, Takahiro Shimada^{**1}, Jie Wang² and Takayuki Kitamura¹

¹Department of Mechanical Engineering and Science, Kyoto University,
Kyoto-Daigaku Katsura, Nishikyo-ku, Kyoto 615-8540, Japan

²Department of Engineering Mechanics, School of Aeronautics and Astronautics, Zhejiang University,
Zheda Road 38, Xihu District, Hangzhou 310027, China

(Received January 24, 2016, Revised March 8, 2016, Accepted March 8, 2016)

Abstract. This work employed density functional theory to investigate the structural and ferroelectric properties of the Ruddlesden-Popper (RP) phase of lead titanate, Pb_2TiO_4 , as well as its phase transitions with epitaxial strain. A wealth of novel structural instabilities, which are absent in the host PbTiO_3 material, were identified in the RP phase through phonon soft-mode analysis. Our calculations showed that the ground state of Pb_2TiO_4 is antiferroelectric, distinct from the dominant ferroelectric phase in the corresponding host material. In addition, applied epitaxial strain was found to play a key role in the interactions among the instabilities. The induction of a sequence of antiferroelectric and antiferrodistortive (AFD) phase transitions by epitaxial strain was demonstrated, in which the ferroic instability and AFD distortion were cooperative rather than competitive, as is the case in the host PbTiO_3 . The RP phase in conjunction with strain engineering thus represents a new approach to creating ferroic orders and modifying the interplay among structural instabilities in the same constituent materials, enabling us to tailor the functionality of perovskite oxides for novel device applications.

Keywords: ferroelectrics; Ruddlesden-Popper phase; antiferroelectricity; strain; first-principles

1. Introduction

Perovskite oxide materials have attracted considerable attention due to their unique dielectric, electrical and magnetic properties, and are thought to have applications in the electronics industry (Lines and Glass 1977). Perovskite structures typically exhibit numerous lattice instabilities, including ferroelectric (FE), antiferroelectric (AFE) and antiferrodistortive (AFD) types. These instabilities generally compete with one another and can significantly affect the macroscopic material properties (Benedek and Fennie 2013). Lead titanate (PbTiO_3) is a typical ferroelectric perovskite oxide that has been the focus of significant research and has been utilized in a variety of electronic devices owing to its outstanding electromechanical properties, large electric polarization and other related characteristics (Shimada *et al.* 2015, Xu *et al.* 2016). PbTiO_3 only exhibits a few unstable soft modes: FE and AFD instabilities. However, AFD distortion in this material is

*Corresponding author, Ph.D. Student, E-mail: xu.tao.44a@st.kyoto-u.ac.jp

**Corresponding author, Assistant Professor, E-mail: shimada@me.kyoto-u.ac.jp

suppressed by the dominant FE instability and does not appear in the bulk FE tetragonal phase. Therefore, PbTiO_3 only undergoes a simple thermally-induced structural transition from the cubic to the tetragonal phase. The ability to control the delicate balance between such instabilities and to create novel ferroic states would be highly advantageous, not only because such control has significant fundamental scientific importance, but also because it would provide a prospective means of achieving novel functionalities.

Recently, significant advances in epitaxial engineering techniques have enabled us to obtain complex layered perovskite phases, such as the Ruddlesden-Popper (RP) phase (Schaak and Mallouk 2002), that not only inherit the properties of the matrix material but also offer a fertile ground for emergent ferroic states and functional modification, such as polarization enhancement (Nakhmanson *et al.* 2005) and hybrid improper ferroelectricity (Oh *et al.* 2015). Inspired by these experimental advances, *ab initio* calculations based on density functional theory have also been extensively applied. Birol *et al.* (2011) studied low n $\text{Sr}_{n+1}\text{Ti}_n\text{O}_{3n+1}$ RP layered perovskites and discovered a rare form of ferroic order. Benedek *et al.* (2011) and Harris (2011) demonstrated hybrid improper ferroelectricity in RP $\text{Ca}_3\text{Ti}_2\text{O}_7$ and $\text{Ca}_3\text{Mn}_2\text{O}_7$ compounds, whose corresponding host materials are nonpolar. Maeno *et al.* (1994, 2001, 2007) systematically explored a $\text{Sr}_{n+1}\text{Ru}_n\text{O}_{3n+1}$ RP series and showed that these materials exhibited fruitful emergent functionalities, including unconventional superconductivity, metamagnetism and magnetic properties, depending on the number of layered cells, n .

Despite its scientific and technological potential, the RP lead titanate homologous series ($\text{Pb}_{n+1}\text{Ti}_n\text{O}_{3n+1}$) remains largely unexplored. Structurally, RP $\text{Pb}_{n+1}\text{Ti}_n\text{O}_{3n+1}$ is composed of stacked PO-terminated PbTiO_3 perovskite [001] slabs, with each slab shifts of $(a/2)$ in the [110] direction. Hence, in contrast to the parent PbTiO_3 perovskite, the TiO_6 oxygen octahedra are obstructed in the [001] direction and only continuously connected in two-dimensional planes, rather than in three dimensions as the host PbTiO_3 material. Since ferroelectric and related structural instabilities originate from the delicate balance between short-range covalent and long-range Coulomb interactions, the original FE phase should be greatly disturbed by this layered structure, so that novel structural phases are expected. A theoretical study aimed at examining ferroelectricity in epitaxially strained Pb_2TiO_4 was recently reported (Fennie and Rabe 2005). However, this study focused only on ferroelectric phases and neglected other structural instabilities, and therefore did not predict the ground state of RP Pb_2TiO_4 and the associated phase transitions with strain are not fully understood.

In the present study, we mapped out all of the structural instabilities and metastable states in RP Pb_2TiO_4 beyond the characteristic unstable modes in PbTiO_3 , with the help of the density functional theory. The ground state of Pb_2TiO_4 in an RP structure was determined to be antiferroelectric, a ferroic state absent in the corresponding host material. In addition, epitaxial strain was found to play a key role in the competition among the instabilities. A sequence of antiferroelectric and antiferrodistortive phase transitions with epitaxial strain was observed, leading to an increase in the number of attainable phases in PbTiO_3 . The layered RP structure evidently allows great flexibility with regard to tailoring the ferroic properties of perovskite materials with unique functionalities.

2. Simulation methods and model

All of the first-principles calculations in the present study were performed using density

functional theory as implemented in the VASP program (Kresse and Hafner 1993). The exchange correction energy was evaluated within the modified Perdew-Burke-Ernzerhof of generalized gradient approximation (GGA-PBESol) (Perdew *et al.* 2008) for solids and surfaces. The employment of GGA-PBESol is rationale and necessary, since this functional has been proved to provide better structural predictions (Shimada *et al.* 2013) compared with the previously used local density approximation (LDA). The electron-ion interactions were described by the projector augmented-wave potentials (Blöch *et al.* 1994), explicitly treating the Pb $5d$, $6s$ and $6p$, the Ti $3s$, $3p$, $3d$ and $4s$, and the O $2s$ and $2p$ electrons as valence states. The electronic wave functions were expanded in plane waves up to a cut-off energy of 500 eV. The present calculations successfully reproduced the structural properties of PbTiO_3 , the host material of the RP Pb_2TiO_4 phase. The lattice constants of tetragonal PbTiO_3 were calculated to be 3.876 and 4.150 Å, which are in excellent agreement with the experimental values of 3.88 and 4.155 Å (Mabud and Glazer 1979) as well as the results reported by other theoretical studies (Shimada *et al.* 2013). Phonon dispersion, with a path including the high symmetry $\Gamma(0,0,0)$, $X(0.5,0,0)$, $M(0.5,0.5,0)$, $Z(0,0,0.5)$ and $A(0.5,0.5,0.5)$ points in the Brillouin zone (BZ), was studied by computing the dynamical matrix, utilizing a finite displacement method in which each ion was displaced by 0.01 Å.

The Pb_2TiO_4 RP contains two structural Pb_2TiO_4 units, characterized by in-plane and out-plane lattice constants a and c , respectively. The epitaxial constraint on a cubic (001)-oriented substrate was simulated by varying the in-plane lattice constraint, a , while allowing the out-of-plane lattice constant, c , to relax. The misfit strain was defined as $\varepsilon = (a - a_0)/a_0$, in which a_0 is the in-plane lattice parameter of stress-free Pb_2TiO_4 . Integrals over the BZ were approximated by sums on a $6 \times 6 \times 2$ Monkhorst-Pack meshes (Monkhorst and Pack 1976). The atomic positions were fully relaxed by the conjugate gradient method until the Hellmann-Feynman force acting on each atom was less than 0.01 eV/Å.

The most common method used for the determination of ground state structures is the classification of the candidate phases followed by the determination of the minimum energy structures for various epitaxial strains. This method is risky in that possible phases may be left out, especially in the case of RP Pb_2TiO_4 , whose structural properties are largely unknown. Herein, we utilized phonon soft-mode analysis through first-principles lattice dynamic calculations to predict the structural properties. We began with full relaxation of the high-symmetry reference RP structure (i.e., the paraelectric phase). The phonon dispersion curve of this structure along the high-symmetry BZ directions was subsequently calculated, from which the unstable phonon soft modes were obtained and used as a guide to search for stabilized structures.

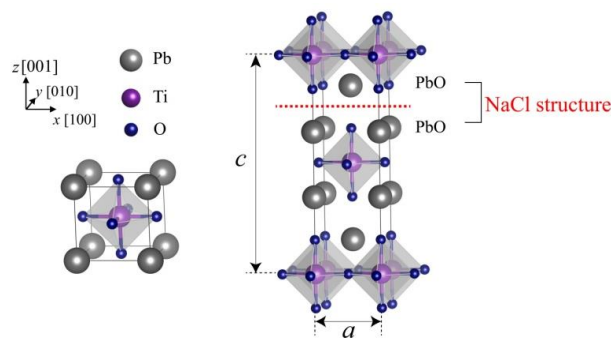


Fig. 1 Crystal structure of the Ruddlesden-Popper compound $\text{Pb}_2\text{Ti}_2\text{O}_4$ in the $I4/mmm$ space group

Based on the calculated phonon band, the real-space eigendisplacements of the unstable modes were frozen, as well as those of their combinations, followed by full structural relaxation and a comparison of the energy of the resultant structures. Following this, we were able to identify one or more dominant unstable modes, readily capable of lowering the energy of the high-symmetry structure and thus likely to contribute to the ground state structure. We then constructed a new starting structure by freezing in these dominant unstable modes. Other unstable modes are incorporated to this new structure to check whether they were able to further reduce the energy, as a means of determining the lowest energy structure. This procedure ensures the accuracy of the final results, although we only consider the energy of structures with single unstable mode or two instabilities to identify the dominant unstable modes. Finally, the phonon calculations were repeated for this lowest energy structure to verify that the candidate ground state structure was really the most stable one.

3. Results and discussion

3.1 Structural instabilities in Ruddlesden-Popper Pb_2TiO_4

The structural properties of RP Pb_2TiO_4 in the high symmetry state were investigated by performing a full optimization of the structure. A body-centered (space group: $I4/mmm$) paraelectric phase with lattice parameters $a_0 = 3.882 \text{ \AA}$ and $c_0 = 12.797 \text{ \AA}$ was obtained, as shown in Fig. 1. These structural parameters are consistent with those previously reported in the literature (Fennie and Rabe 2005), indicating that the present calculations provide reliable results.

We then calculated the phonon dispersion curve of stress-free high symmetry RP Pb_2TiO_4 , with particular attention to the unstable modes. The phonon bands and frequencies at the high symmetry points of the Brillouin zone are shown in Fig. 2 and Table 1, respectively. One can see that the Pb_2TiO_4 exhibits structural instabilities at all the sampled k points, as indicated by the negative (imaginary) frequencies, and displays a much richer set of structural instabilities than the corresponding host PbTiO_3 . The dominant instability, with an imaginary frequency of $141i$, is located in the zone-center ($\Gamma(0,0,0)$). This unstable phonon has a doubly degenerate E_u symmetry.

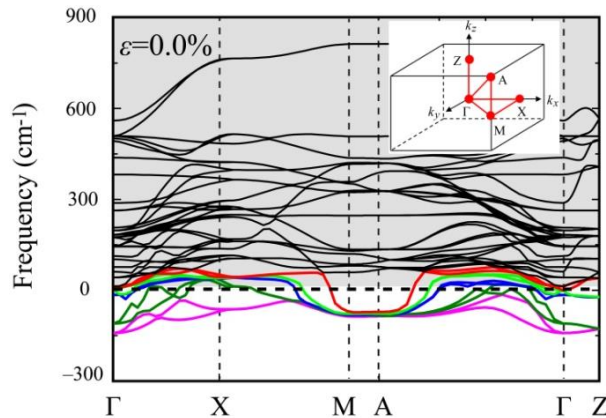


Fig. 2 Phonon bands calculated at the high-symmetry points of the Brillouin zone for $I4/mmm$ Pb_2TiO_4 in the stress-free state. Negative values denote imaginary frequencies

Table 1 Soft-phonon frequencies at Γ , X , M , A and Z for stress-free Pb_2TiO_4

$\Gamma(0,0,0)$		$X(0.5,0,0)$		$M(0.5,0.5,0)$		$A(0.5,0.5,0.5)$		$Z(0,0,0.5)$	
Label	w	Label	w	Label	w	Label	w	Label	w
E_u ($\text{AFE}_{x,y}$)	$141i$	B_1 (AFE_z)	$63i$	B_{1g} ($\text{AFD}_{x,y}$)	$87i$	E ($\text{AFD}_{x,y}$)	$85i$	E ($\text{AFE}_{x,y}$)	$127i$
E_u ($\text{FE}_{x,y}$)	$110i$			B_{3u} ($\text{FE}_{(h-h)}$)	$83i$	E ($\text{FE}_{(h-h)}$)	$77i$	E ($\text{AFE}_{x,y}$)	$23i$
				B_{3g} ($\text{AFD}_{x,y}$)	$82i$	A_2 (AFD_z)	$71i$		
				B_{1u} ($\text{FE}_{(h-h)}$)	$77i$				
				B_{2g} (AFD_z)	$73i$				

Visualization of the eigenvectors of these modes identify them as AFE in character (see Fig. 3(a)): Pb and Ti cations move against oxygen octahedral along the $[100]$ or $[010]$ directions, and this movement is antiparallel with respect to neighboring atomic planes. Since the linear combination of the degenerate modes can lead to numerous equivalent eigendisplacements, we considered two special cases with distortions along the $[100]$ and $[110]$ directions. Freezing-in these modes separately, we obtain two different structures with space group $Pmnm$ and $Cmcm$ for the distortions along the $[100]$ and $[110]$ directions, respectively. The energy of the $Pmnm$ structure was lower than that of the $Cmcm$ by 0.4 eV, and therefore, we considered only the $Pmnm$ structure (AFE_x) in the following. The second-lowest frequency mode at $\Gamma(0,0,0)$ is also a two-dimensional E_u mode with an imaginary frequency of $110i$, indicative of instability. This unstable mode is doubly degenerate and corresponds to Pb and Ti atoms in both slabs moving against their oxygen cages along the $[100]$ or $[010]$ directions, thus corresponding to ferroelectric instabilities

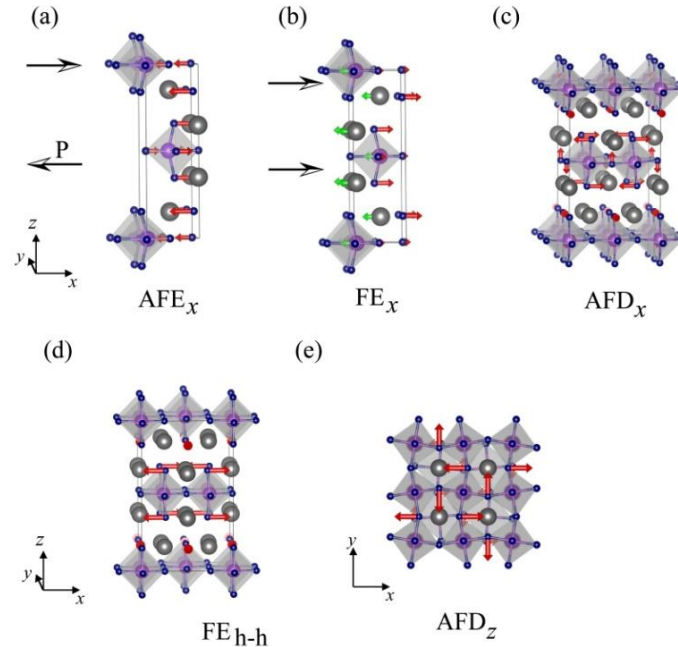


Fig. 3 The displacement patterns of typical unstable modes in the BZ of (a and b) $\Gamma(0,0,0)$ and (c, d and e) $A(0.5, 0.5, 0.5)$

(see Fig. 3(b)). Similarly, we also considered distortion along the [100] and [110] directions, and freezing-in the [110] FE distortion led to a higher energy than the [100] FE distortion. Therefore, we considered only the [100] FE distortion. Freezing-in the mode with [100] direction polarization and performing relaxation, we obtained a structure with space group $I2mm$ for which $a=4.011 \text{ \AA}$, $b=3.849 \text{ \AA}$ and $c=12.836 \text{ \AA}$. In this structure, the spontaneous polarization is $81 \mu\text{C}/\text{cm}^2$ along the [100] direction, comparable to that of the bulk PbTiO_3 . It should be noted that the frequency of the FE_z distortion is highly positive, indicating that the rock salt-type inserts suppress polarization along the [001] direction.

Point A (0.5, 0.5, 0.5) also exhibits numerous structural instabilities. The strongest one (lowest frequency) has quadruple degenerate modes that transform according to the irreducible representation E , characterized by AFD distortion. This degenerate AFD distortion can be described by $a^0b^0c^0$ (AFD_x) and $a^0b^0c^0$ (AFD_y) in Glazer tilt patterns (Glazer 1972) that occur within two neighboring Pb_2TiO_4 perovskite slabs (see Fig. 3(c)). The slightly higher frequency mode is also an E mode. The real-space eigendisplacement of this unstable mode consists of Ti and O atoms moving against one another in the xy plane, showing in-plane head-to-head polarization (see Fig. 3(d)). The final mode is A_2 , with an imaginary frequency of $71i$. This doubly degenerate unstable mode exhibits $a^0b^0c^{-1}$ AFD order (AFD_z) with an out-of-plane rotation axis (see Fig. 3(e)). Additional instability characteristics associated with other points, including FE and AFE, are listed in Table 1, together with their symmetry labels and associated imaginary frequencies. These instabilities have never been observed in bulk PbTiO_3 , and may possibly lead to a rich variety of phase diagrams.

3.2 Ground state structure determination

With these structural instabilities in mind, we investigated combinations of these unstable modes to determine the ground state of RP Pb_2TiO_4 . We computed the energies of configurations constructed from combinations of the eigenvectors of any two unstable modes, in anticipation of a variety of low-energy metastable structures. The relative energy values of the resultant structures after full relaxation as well as those of freezing-in a single mode (located in the diagonal section) are summarized in Table 2, in which the high symmetry $I4/mmm$ phase is set as the reference state. It is evident that some modes are collaborative, coexisting and lowering the total energy when combined, such as the AFD_x and AFD_z modes, while other pairs compete with one another, such that the total energy is increased or one mode is completely suppressed. Particularly, the AFE_x distortion in the $\Gamma(0,0,0)$ plays a dominant role in the structural instability, as it suppresses all the

Table 2 Relative energy values (eV) for RP Pb_2TiO_4 structures upon freezing-in one and two unstable modes in the stress-free state. The paraelectric phase is set as the reference state

$\varepsilon = 0.0\%$	AFE_x	FE_x	AFE_z	$\text{AFD}_{x,y}$	$\text{FE}_{(h-h)}$	AFD_z
AFE_x	-0.660					
FE_x	AFE_x	-0.166				
AFE_z	AFE_x	FE_x	-0.022			
$\text{AFD}_{x,y}$	AFE_x	FE_x	-0.103	-0.104		
$\text{FE}_{(h-h)}$	AFE_x	-0.197	-0.045	$\text{AFD}_{x,y}$	-0.042	
AFD_z	AFE_x	-0.156	-0.099	-0.182	-0.197	-0.101

other modes, and the relative energy of the AFE_x distortion is -0.66 eV, a value that is much lower than that of other single or combined unstable modes. These results are reasonable since the lowest phonon frequencies are associated with the AFE mode. Due to its pronounced ability to reduce the overall energy, the AFE_x distortion should play a role in determining the ground state of the RP Pb_2TiO_4 structure. Having identified the dominant distortion, other soft modes were incorporated into the $Pmnm$ structure along with AFE_x distortion to determine whether or not they further reduced the energy of the system. However, relaxation of the initial structure always yielded a state containing only AFE_x distortion. Thus, the minimum energy structure of RP Pb_2TiO_4 is a $Pmnm$ phase characterized by AFE_x distortion. Phonon calculations were subsequently repeated for this $Pmnm$ structure. The phonon bands of the RP $Pmnm$ Pb_2TiO_4 showed no existing lattice instabilities in the BZ, suggesting that the $Pmnm$ AFE structure is indeed the ground state of RP Pb_2TiO_4 in the stress-free state, contrary to the FE phase in the $PbTiO_3$. The large energy difference between this ground state and the high symmetry phase (-0.66 eV) suggests that the $Pmnm$ AFE structure may be easily produced experimentally under appropriate synthetic process.

It is noteworthy that the lead $6s$ and O $2p$ states in the neighboring slabs of Pb_2TiO_4 RP are strongly hybridized as the case in ferroelectric $PbTiO_3$, which plays important role in stabilizing the AFE distortion. The hybridization in this ground state is much stronger than that in $I2mm$ phase with FE distortion, hence the AFE distortion is stabilized over the FE distortion in Pb_2TiO_4 RP. The calculated lattice parameters were $a=4.20$ Å, $b=3.85$ Å and $c=12.33$ Å. The spontaneous polarization in each slab was calculated to be 128 $\mu C/cm^2$ along the $[100]$ direction, a value that was larger than that of the corresponding host $PbTiO_3$, although the macroscopic polarization was zero due to the characteristics of AFE distortion.

Table 3 Relative energy values (eV) for RP Pb_2TiO_4 structures upon freezing-in one and two unstable modes at a strain of $\varepsilon=-1.5\%$. The paraelectric phase is set as the reference state

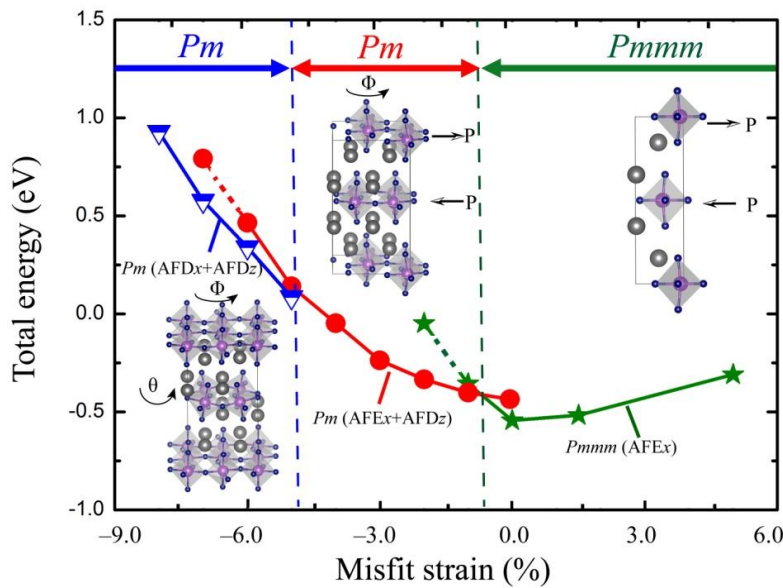
$\varepsilon=-1.5\%$	AFE_x	AFD_z	$AFD_{x,y}$	AFE_z	$FE_{(h-h)}$	FE_x
AFE_x	-0.285					
AFD_z	-0.435	-0.179				
$AFD_{x,y}$	AFE_x	-0.303	-0.071			
AFE_z	AFE_x	-0.175	-0.102	-0.036		
$FE_{(h-h)}$	AFE_x	-0.271	$AFD_{x,y}$	-0.048	-0.022	
FE_x	AFE_x	-0.273	$AFD_{x,y}$	-0.063	FE_x+AFD_z	-0.052

Table 4 Relative energy values (eV) for RP Pb_2TiO_4 structures upon freezing-in one and two unstable modes at a strain of $\varepsilon=-3.0\%$. The paraelectric phase is set as the reference state

$\varepsilon=-3.0\%$	AFE_x	AFD_z	$AFD_{x,y}$	AFE_z	$FE_{(h-h)}$	FE_x
AFE_x	-0.204					
AFD_z	-0.561	-0.408				
$AFD_{x,y}$	-0.130	-0.507	-0.113			
AFE_z	-0.222	-0.407	-0.132	-0.089		
$FE_{(h-h)}$	AFE_x	-0.465	$AFD_{x,y}$	-0.200	-0.033	
FE_x	AFE_x	AFD_z	$AFD_{x,y}$	-0.097	-0.037	-0.052

Table 5 Relative energy values (eV) for RP Pb_2TiO_4 structures upon freezing-in one and two unstable modes at a strain of $\varepsilon=-5.0\%$. The paraelectric phase is set as the reference state

$\varepsilon=-5.0\%$	AFD _z	AFE _z	FE _z	AFD _{x,y}	AFE _x	FE _x
AFD _z	-0.844					
AFE _z	AFD _z	-0.235				
FE _z	AFD _z	-0.278	-0.518			
AFD _{x,y}	-0.950	-0.307	AFD _{x,y}	-0.204		
AFE _x	-0.905	-0.527	-0.417	AFD _{x,y}	-0.157	
FE _x	-0.847	-0.236	FE _z	AFD _{x,y}	AFD _{x,y}	-0.077

Fig. 5 Crystal phase diagram for RP Pb_2TiO_4 under epitaxial strain. The total energy of the PbTi_2O_4 in the $I4/mmm$ space group is set to zero

Due to the highly dominant and exclusive role of AFE_x distortion in the unstrained state, as well as its tendency to soften with increasing strain, it is natural to consider combinations of the AFE_x mode with other distortions as potential stable structures under tensile strain. Nevertheless, within the range of epitaxial strain examined, the combined frozen-in distortions were found to disappear after relaxation in favor of an AFE_x phase, just as in the case of the unstrained state. As the compressive strain was increased, the AFE_x mode stiffened, such that the AFE_x distortion was compatible with other distortions and the ground state was replaced with other single or combined distortions. The transition point was located at a strain of approximately $\varepsilon=-0.2\%$, at which point the AFE_x and AFD_z distortions coexisted and the material was more stable than in the case of a single AFE_x mode, even though the lowest frequency mode was still the AFE_x distortion. Thus, the stable RP Pb_2TiO_4 structure at epitaxial strains greater than -0.2% is a $Pmnm$ phase with AFE_x distortion.

As the strain was decreased, the competition between various unstable modes was modified and the dominant instability changed from the AFE_x to the AFD_z mode in terms of phonon frequencies

at a strain of approximately -1.5% . Therefore, we can conclude that the ground state in the strain range of -0.2% to -1.5% is AFE_x distortion combined with one or more other distortions, while the ground state at greater compressive strains is AFD_z distortion mixed with other modes. This conclusion is validated by the total energies of structures with two frozen-in distortions under strains of -1.0% and -3.0% , as shown in Tables 3 and 4. In the case of -1.0% strain, the frozen AFD_z distortion minimized the structural energy and further incorporation of other instabilities were degenerate to this single AFD_z distortion, except for the AFE_x distortion, which coexisted with the original AFD_z mode and generated a Pm structure. These results demonstrate that the AFD and AFE distortions, unlike the AFD and FE degrees of freedom in bulk $PbTiO_3$, collaborate rather than compete with one another, leading to the lowest energy state of the RP Pb_2TiO_4 under this compressive strain. In this Pm ground state, the calculated AFD_z distortion was 29° and the polarization in each slab was $54 \mu C/cm^2$. The application of a -3.0% strain produced a similar trend, such that the AFD_z mode combined with the AFE_x mode generated the most stable structure. Other strain points were also sampled (-1.5 , -2.0 and -4.0%) and the results turned out to be similar. After carefully assessing the effects of increasing compressive strain, we determined a transition strain of approximately -4.2% , at which point the combined AFD_z and AFD_x distortions became more stable. Thus, it appears that the ground state of Pb_2TiO_4 is associated with a combination of the AFE_x and AFD_z distortions at intermediate compressions ranging from -0.2 to -4.2% .

Employing the same procedure as described above, we investigated the stable structures of RP Pb_2TiO_4 under severe compression ($\epsilon=-5.0\%$). At this level of compressive strain, the lowest frequency mode was the AFD_z distortion ($215i$), followed by AFE_z distortion with an imaginary frequency of $182i$. In addition, the FE_z , AFD_x and AFE_x soft modes also exhibited low frequency values ($112i$, $89i$ and $87i$, respectively), while the last soft mode was FE_x distortion ($33i$). The energies of configurations with frozen these modes as well as their combinations are presented in Table 5. These results demonstrate that the interplay between the two strongest modes (AFD_z and AFE_x) is competitive and that the AFE_z mode is suppressed when these two are combined. However, the AFD_z and AFD_x modes are cooperative and their combination leads to the lowest energy state. We then add other instabilities separately as well as all together to this low energy configuration to examine their roles in stabilizing the structure. In each case, the resulting structures relaxed to yield a Pm symmetry phase. Further increases in the misfit strain also generated a lowest energy structure with AFD_z and AFD_x distortions, consistent with the dominant nature and softening trend of the AFD_z mode. Thus, the ground state of RP Pb_2TiO_4 under high compressions ($\epsilon>-4.2\%$) is associated with the AFD_z mode combined with AFD_x distortion.

Based on the above results, the complete phase diagram of RP Pb_2TiO_4 is presented in Fig 5. Here it is evident that, over the range of tensile strain to slightly compressive strain ($\epsilon=-0.2\%$), the most energetically favorable Pb_2TiO_4 RP phase is in the $Pmnm$ space group characterized by AFE_x distortion, a novel ferroic order in the host $PbTiO_3$ material. With increasing compressive strain, the total energy of the $Pmnm$ structure increases and the Pm structure becomes the lowest energy structure, in which the ferroic instability (AFE_x) and AFD distortion (AFD_z) are collaborative and act to stabilize the structure. In the case of a large compressive strain ($\epsilon>-4.2\%$), the nonpolar Pm structure with AFD_z and AFD_x distortions turns into the ground state. Interestingly, this sequence of structural transitions is completely different from that of the host $PbTiO_3$ material.

4. Conclusions

First-principles calculations based on DFT were employed to investigate the structural and ferroelectric properties of the layered oxide RP Pb_2TiO_4 , as well as the phase transitions under applied misfit strains. The results show that the presence of rock salt-type inserts in the RP structure significantly changes the structural instabilities and ferroic orders of the host bulk PbTiO_3 crystal. RP Pb_2TiO_4 displays a variety of novel structural degree of freedoms, including FE, AFE and AFD types. The structural ground state of Pb_2TiO_4 was determined to be the AFE phase, which has not been identified to that in bulk PbTiO_3 . RP Pb_2TiO_4 undergoes a succession of AFE and AFD phase transitions mediated by epitaxial strain, in which the ferroic instability and AFD distortion are cooperative rather than competitive as is the case in the host PbTiO_3 . These AFD distortions are hidden and suppressed by the dominant FE instability in PbTiO_3 . Therefore, the RP phase not only creates novel ferroic orders but also significantly affects the interplay among the instabilities in the same constituent material. The strain and RP phase engineering thus represent new approaches to controlling ferroic orders and tailoring functionalities within the same perovskite oxide materials.

Acknowledgments

This work was supported in part by JSPS KAKENHI Grants, numbers 25000012, 26289006 and 15K13831.

References

- Benedek, N.A. and Fennie, C.J. (2011), "Hybrid improper ferroelectricity: A mechanism for controllable polarization-magnetization coupling", *Phys. Rev. Lett.*, **106**(10), 107204.
- Benedek, N.A. and Fennie, C.J. (2013), "Why are there so few perovskite ferroelectrics?", *J. Phys. Chem. C.*, **117**, 13339-13349.
- Biol, T., Benedek, N.A. and Fennie, C.J. (2011), "Interface control of emergent ferroic order in Ruddlesden-Popper $\text{Sm}_{n+1}\text{Ti}_n\text{O}_{3n+1}$ ", *Phys. Rev. Lett.*, **107**(25), 257602.
- Blöchl, P.E. (1994), "Projector augmented-wave method", *Phys. Rev. B.*, **50**(24), 17953.
- Ceperley, D.M. and Alder, B.J. (1980), "Ground state of the electron gas by a stochastic method", *Phys. Rev. Lett.*, **45**(7), 566.
- Fennie, C.J. and Rabe, K.M. (2005), "First-principles investigation of ferroelectricity in epitaxially strained Pb_2TiO_4 ", *Phys. Rev. B.*, **71**(10), 100102.
- Fobes, D., Yu, M.H., Zhou, M., Hooper, J., O'Connor, C.J., Rosario, M. and Mao, Z.Q. (2007), "Phase diagram of the electronic states of trilayered ruthenate $\text{Sr}_4\text{Ru}_3\text{O}_{10}$ ", *Phys. Rev. B.*, **75**(9), 094429.
- Glazer, A.M. (1972), "The classification of tilted octahedra in perovskites", *Acta Crystallogr. B.*, **28**(11), 3384-3392.
- Harris, A.B. (2011), "Symmetry analysis for the Ruddlesden-Popper systems $\text{Ca}_3\text{Mn}_2\text{O}_7$ and $\text{Ca}_3\text{Ti}_2\text{O}_7$ ", *Phys. Rev. B.*, **84**(6), 064116.
- Kresse, G. and Hafner, J. (1993), "Ab initio molecular dynamics for liquid metals", *Phys. Rev. B.*, **47**(1), 558.
- Lines, M.E. and Glass, A.M. (1997), "Principles and applications of ferroelectrics and related materials", Oxford University Press, New York, U.S.A.
- Mabud, S.A. and Glazer, A.M. (1979), "Lattice parameters and birefringence in PbTiO_3 single crystals", *J. Appl. Crystallogr.*, **12**(1), 49-53.
- Maeno, Y., Hashimoto, H., Yoshida, K., Nishizaki, S., Fujita, T., Bednorz, J.G. and Lichtenberg, F. (1994),

- “Superconductivity in a layered perovskite without copper”, *Nat.*, **372**(6506), 532-534.
- Monkhorst, H.J. and Pack, J.D. (1976), “Special points for brillouin-zone integrations”, *Phys. Rev. B.*, **13**(12), 5188.
- Nakhmanson, S.M., Rabe, K.M. and Vanderbilt, D. (2005), “Polarization enhancement in two-and three-component ferroelectric superlattices”, *Appl. Phys. Lett.*, **87**(10), 102906.
- Oh, Y.S., Luo, X., Huang, F.T., Wang, Y. and Cheong, S.W. (2015), “Experimental demonstration of hybrid improper ferroelectricity and the presence of abundant charged walls in (Ca, Sr) 3Ti2O7 crystals”, *Nat. Mater.*, **14**(4), 407-413.
- Perdew, J.P., Ruzsinszky, A., Csonka, G.I., Vydrov, O.A., Scuseria, G.E., Constantin, L.A., Zhou, X. and Burke, K. (2008), “Restoring the density-gradient expansion for exchange in solids and surfaces”, *Phys. Rev. Lett.*, **100**(13), 136406.
- Perry, R.S., Galvin, L.M., Grigera, S.A., Capogna, L., Schofield, A.J., Mackenzie, A.P., Chiao, M., Julian, S.R., Ikeda, S.I., Nakatsuji, S., Maeno, Y. and Pfleiderer, C. (2001), “Metamagnetism and critical fluctuations in high quality single crystals of the bilayer ruthenate Sr3Ru2O7”, *Phys. Rev. Lett.*, **86**(12), 2661.
- Schaak, R.E. and Mallouk, T.E. (2002), “Perovskites by design: A toolbox of solid-state reactions”, *Chem. Mater.*, **14**(4), 1455-1471.
- Shimada, T., Ueda, T., Wang, J. and Kitamura, T. (2013), “Hybrid hartree-fock density functional study of charged point defects in ferroelectric PbTiO3”, *Phys. Rev. B.*, **87**(17), 174111.
- Shimada, T., Wang, J., Ueda, T., Uratani, Y., Arisue, K., Mrovec, M., Elsasser, C. and Kitamura, T. (2015), “Multiferroic grain boundaries in oxygen-deficient ferroelectric lead titanate”, *Nano Lett.*, **15**(1), 27-33.
- Xu, T., Shimada, T., Araki, Y., Wang, J. and Kitamura, T. (2016), “Multiferroic domain walls in ferroelectric PbTiO3 with oxygen deficiency”, *Nano Lett.*, **16**(1), 454-458.

DC